Improved battery storage systems modeling for predictive energy management applications

Ricardo Silva, Clara Gouveia, Leonel Carvalho, Jorge Pereira
INESC TEC, Institute for Systems and Computer Engineering
Porto, Portugal
ricardo.emanuel@inesctec.pt, clara.s.gouveia@inesctec.pt, leonel.carvalho@inesctec.pt, jpereira@inesctec.pt

***Abstract*— This paper presents a model predictive control (MPC) framework for battery energy storage systems (BESS) management considering models for battery degradation, system efficiency and V-I characteristics. The optimization framework has been tested for both microgrids and hybrid parks with different renewable generation and load mix considering several operation strategies. A comparison for one-year simulations between the proposed model and a naïve BESS model, show an increase in computation times that still allows the application of the framework for real-time control. Furthermore, a tradeoff between financial revenue and reduced BESS degradation was evaluated for the yearly simulation, considering the degradation model proposed. Results show that a conservative BESS usage strategy can have a high impact on the asset's lifetime and on the expected system revenues, depending on factors such as the objective function, system, and degradation cost considered.**

***Index Terms*—Battery degradation, battery energy storage systems, linear model, microgrid, model predictive control.**

NOMENCLATURE

Indices and sets	
$t \in T$	Set of time intervals within the optimization horizon.
$z \in Z$	Set of trapeziums approximating the P-Q capability curve.
$s \in S$	Set of piecewise segments approximating the BESS efficiency curve.
Parameters	
$\hat{\eta}^{b,+}, \hat{\eta}^{b,-}$	BESS charge/discharge efficiency.
Δt	Length of the optimization time step [h].
$\overline{\varepsilon}^{b}(.), \underline{\varepsilon}^{b}(.)$	BESS dynamic maximum/minimum energy content [Wh].
$\overline{E}^{b}, \underline{E}^{b}$	BESS absolute maximum/minimum energy content [Wh].
$\hat{\lambda}_t^{mk}, \hat{\lambda}_t^{fi}$	Forecasted market prices/feed-in tariffs for t [€/Wh].
$\hat{P}_t^{G}$	Forecasted RES generation during t [W].
$\overline{P}^{G,cut}$	Maximum curtailable RES capacity [W].
$\overline{P}^{b,+}, \overline{P}^{b,-}$	BESS charge/discharge power rate limit [W].
$\hat{P}_z^{tr,l}, \hat{P}_z^{tr,r}$	Active power coordinate at the left/right upper corner of the z^{th} trapezium [W].
$\hat{Q}_z^{tr,l}, \hat{Q}_z^{tr,r}$	Reactive power coordinate at the left/right upper corner of the z^{th} trapezium [var].
$\hat{P}_t^{L}$	Forecasted load demand during t [W].
$\overline{P}_s^{b,+}, \overline{P}_s^{b,-}$	BESS maximum charge/discharge power rate limit for segment s [W].
$\underline{P}_s^{b,+}, \underline{P}_s^{b,-}$	BESS minimum charge/discharge power rate limit for segment s [W].
Variables	
e_t^{b}	BESS energy content at the end of t [Wh].
Δe_t^{b}	Change in BESS energy content in t as a result of the applied power $p_t^{b,+/-}$ [Wh].
$p_t^{b,+}, p_t^{b,-}$	BESS charge/discharge setpoint during t [W].
e_t^{deg}	Battery's degraded capacity at the end of t [Wh].
p_t^{abs}, p_t^{inj}	Absorption/injection setpoint at the PCC during t [W].
$\Delta e_t^{+}, \Delta e_t^{-}$	Positive/negative energy imbalance at t [Wh].
$p_t^{G,cut}$	RES curtailment setpoint during t [W].
$\delta_t^{PCC}, \delta_t^{b}$	Binary variables to avoid simultaneous inverse power flows during t.
$p_{z,t}^{b,tr}, q_{z,t}^{b,tr}$	BESS active/reactive discharge setpoint, within trapezium z, during t [W].
$\delta_{z,t}^{b,tr}$	Binary variable for activating a single trapezium area during t.
e_t^{DA}, e_t^{PCC}	Energy scheduled/effectively injected (< 0)/ absorbed (≥ 0) at the PCC, during t [W].
$p_t^{L,cut}$	Load curtailment setpoint during t [W].
δ_t^{L}	Binary variable indicating the curtailed status of the load asset (0: curtailed) during t.
$z_{t,s}^{b,+}, z_{t,s}^{b,-}$	BESS charge/discharge setpoint (DC side) in the s^{th} line segment, during t [W].
$p_{t,s}^{b,+}, p_{t,s}^{b,-}$	BESS charge/discharge setpoint (AC side) in the s^{th} line segment, during t [W].
$\delta_{t,s}^{b,+}, \delta_{t,s}^{b,-}$	Binary variable for enabling BESS charge/discharge within segment s, during t.

I. INTRODUCTION

The operation of renewable-based power systems increasingly relies on the optimal exploitation of battery energy storage systems (BESS) and flexible loads. Optimal scheduling of BESS has been widely covered in literature, integrated for example in microgrids, energy communities and renewable power generation plants. The use of model predictive control (MPC) as, for example, showed in [1], presents an adequate framework for real-time, on-line scheduling of BESS, being able to compensate at each time step for real-time disturbances or forecast errors.

In most cases, a simplified BESS modelling approach is considered, adopting constant battery charging/discharging powers and efficiency. This naïve model can be found on several recent papers approaching an optimal BESS control strategy [2]–[10]. A review performed over optimization strategies concerning BESS [11] highlights this tendency. In addition, and apart from references [9] and [10], the impact of the operation strategy selected in the battery's lifetime is typically neglected. In [12], the authors have tested the impact of modelling battery dynamics and electrochemical degradation in the optimal control strategy of BESS, demonstrating that a simplified model could, although, lead to an erroneous techno-economic performance assessment.

This paper proposes an enhanced BESS modelling approach for an MPC framework, that aims at balancing computational tractability with accuracy, based on three fundamental characteristics: battery degradation, system efficiency and V-I characteristics. To the extent of our knowledge, no other work has proposed such a complete and tractable model, applicable to Mixed Integer Linear Programming (MILP) formulations. Considering this framework, an analysis is performed over the impact of adopting distinct BESS usage strategies on different systems and objective functions.

II. BESS LINEAR MODEL

A linear model of BESS is considered, specifically designed for Li-ion technologies, and focused on three fundamental characteristics: V-I characteristics, system efficiency and degradation.

A. V-I characteristics

We adapted the model presented at [13] (recently described as the C/L/C model at [14]), that adds to the MILP formulation the possibility to adjust the battery energy content limits as a function of the power setpoints' magnitude imposed at each time step. The definition of dynamic energy content limits, $\underline{\varepsilon}^b(.)$ and $\overline{\varepsilon}^b(.)$, stems from the fact that the battery cannot charge or discharge completely (i.e., reach the absolute, static, energy content limits, $\underline{E}^b$ and $\overline{E}^b$) when subjected to high charge and discharge currents, respectively, due to the voltage spike/drop associated. These limits represent the energy content of the battery when its voltage limits are reached, being more restrictive when higher discharge or charge currents are applied, respectively. We establish therefore the chain of magnitude $\underline{E}^b \le \underline{\varepsilon}^b\left(\frac{p_t^b}{\hat{V}^{N,-}}\right) \le e_t^b \le \overline{\varepsilon}^b\left(\frac{p_t^b}{\hat{V}^{N,+}}\right) \le \overline{E}^b$. The definition of the BESS nominal charge ($\hat{V}^{N,+}$) and discharge ($\hat{V}^{N,-}$) voltages, along with the parameters for $\underline{\varepsilon}^b(.)$ and $\overline{\varepsilon}^b(.)$ linearization (slopes $\hat{m}^{b,+/-}$ and origins $\hat{o}^{b,+/-}$) can be achieved through a combination of the manufacturer's information and relatively simple tests, whose methodology can be consulted at [13].

B. System efficiency

Since the BESS inverters' efficiency is nonlinear for small output powers (see Fig. 1), we defined a 2-step piecewise model that linearly approximates the charge and discharge efficiency curves for output powers below and above an empirical threshold (10%) of the inverter's rated power. The parameters for the first line segment (slopes $\hat{m}^{\eta,+/-}$ and origins $\hat{o}^{\eta,+/-}$), are obtained by performing a least squares approximation of the available test values below the rated power's threshold. In order to embed this model in the MILP, the line parameters for charging and discharging must be obtained for different curves than the one depicted in Fig. 1: the line's abscissa corresponds to the rated power intervals $]0, 0.1 \times \overline{P}^{b,+}]$ and $]0, 0.1 \times \overline{P}^{b,-}]$, respectively; the line's ordinates to the DC-side power setpoints from the experimental trials, $P^{b,+} \times \hat{\eta}^{b,+}(P^{b,+})$ and $\frac{P^{b,-}}{\hat{\eta}^{b,-}(P^{b,-})}$, respectively. This linear approach converts an AC to a DC-side power setpoint, avoiding a non-linearity that would result from multiplying the calculated efficiencies by the AC-side power setpoints. The second segment is obtained by averaging the observed efficiencies for values above the 10% threshold. This segment is then extended backwards until the intersection point with the first one, avoiding possible large discontinuities in the vicinity of the threshold. Equation (1) is used to obtain this new power threshold between segments, either for charging or discharging.

$$\overline{P}_{s=1}^{b,+/-} = \underline{P}_{s=2}^{b+/-} = \frac{\left(\hat{\eta}^{b+/-} \times 0.1 \times \overline{P}^{b,+/-} - \hat{o}^{\eta,+/-}\right)}{\hat{o}^{\eta,+/-}}. \quad (1)$$

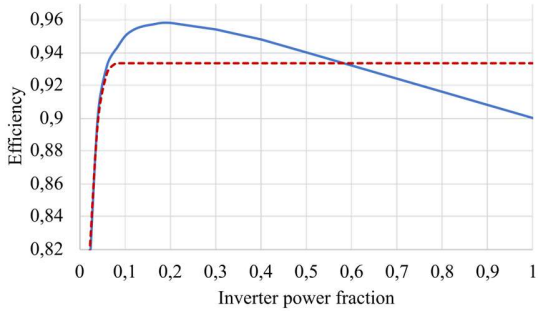

Figure 1. Typical inverter's charge efficency curve (adapted from [15]). The two-step piecewise linearization proposed is depicted in dashed red.

C. Degradation

BESS degradation can be accounted for by limiting its total allowed value within the optimization's horizon, based on the discharging cycles imposed. Starting from the battery's

Submitted to the 22nd Power Systems Computation Conference (PSCC 2022).

degradation curve provided by the manufacturer (Fig. 2), which relates the depth of discharge (DOD) with the total number of cycles until the end-of-life (EOL) criterion is met (e.g., 70% of the initial battery's capacity $\hat{E}^{b,N}$) a relationship is established between DOD and the corresponding percentage of cycle life loss (i.e., loss of storage capacity; see Fig. 3). The conversion between curves is performed by applying (2). The cycle life loss curve is linearized by a least squares' approximation, forcing it to intersect the origin. The line's slope $\hat{m}^{deg}$ is used to estimate the degradation caused by each discharge cycle using (3). The EOL criterion can then be used to define the maximum daily capacity degradation value $\overline{E}^{deg}$, using (4).

$$Cycle\ life\ loss\ (DOD) = \frac{100-EOL}{Number\ of\ cycles(DOD)} \quad (2)$$

$$e_t^{deg} = \hat{m}^{deg}\ \frac{p_t^-}{\hat{\eta}^{b,-}},\ e_t^{deg} \in \mathbb{R}_0^+ \quad (3)$$

$$\overline{E}^{deg} = \frac{(100 \quad)\hat{E}^{b,N}}{100\times365}. \quad (4)$$

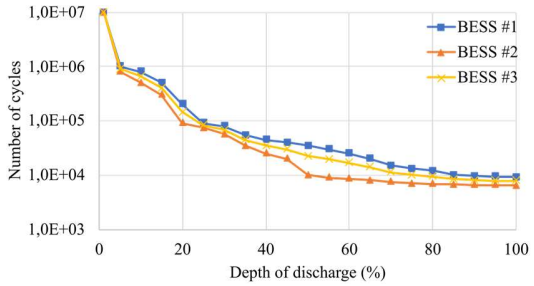

Figure 2. Typical manufacturer's degradation curves for Li-ion batteries.

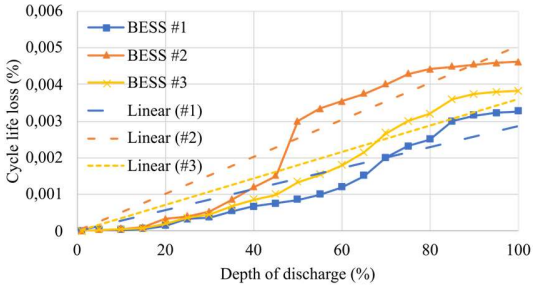

Figure 3. Cycle life loss curves resulting from adapting the curves in Fig. 2. A depiction of each curve's linearization is provided as dashed lines.

III. Predictive Energy Management Algorithm

This section describes the proposed optimal operation scheduling algorithm for BESS, consisting of a MILP problem adapted for different objective functions and for the system to which the BESS is connected (e.g., a microgrid (MG) or a wind-solar hybrid park (HP)), that can include different types of renewable energy sources' (RES) generation and load assets. The algorithm is aimed at running in real-time, based on an MPC framework. The provided outputs include the BESS active and reactive power schedules and setpoints for renewable generation and load curtailment, when required. For the sake of simplicity, the equations presented assume a single aggregated representation per asset type (renewable generation, load demand and BESS) but can easily be adapted to consider multiple assets per type.

The general formulation considers 2 different objective functions: price arbitrage (OF1, (5)) and minimizing energy deviations (OF2, (6)), from a previous (day-ahead) schedule.

$$Min \sum_{t\in T}\left(p_t^{abs}\hat{\lambda}_t^{mk} - p_t^{inj}\hat{\lambda}_t^{fi} + p_t^{L,cut}\hat{\lambda}^{L,cut}\right)\Delta t \quad (5)$$

$$Min \sum_{t\in T}\left(\Delta e_t^- + \Delta e_t^+ + p_t^{L,cut}\hat{\lambda}^{L,cut}\right) \quad (6)$$

Note that when $\Delta e_t^{\Delta,-} > 0$ there is a deficit of injected energy regarding the day-ahead scheduled value for time step t. On the other hand, if $\Delta e_t^{\Delta,+} > 0$, there is an excess of injected energy. Both are penalized in (6). When considering demand (for MG), the inclusion of a cost for load curtailment ($\hat{\lambda}^{L,cut}$) aims at discouraging its usage. Conversely, if this cost is smaller than $min\ (\hat{\lambda}_t^{mk})$, then this mechanism is preferred over grid import.

The constraints applied in the general formulation include: (7), an equilibrium equation; (8) to limit, when applicable, RES curtailment; (9) and (10) to limit power throughput rates at the BESS; (11) to update the energy content of the BESS between steps ($\hat{e}^{b,0}$ is the BESS initial energy content); and (12) to bound that energy content within the battery's limits. If the objective function chosen is (6), then (13) and (14) must also be added to calculate the energy imbalances.

$$p_t^{abs} - p_t^{inj} = p_t^{b,+} - p_t^{b,-} - \hat{P}_t^G + p_t^{G,cut} + \hat{P}_t^L - p_t^{L,cut},$$
$$\forall\ t \in T, p_t^{abs}, p_t^{inj} \in \mathbb{R}_0^+ \quad (7)$$

$$p_t^{G,cut} \le \overline{P}^{G,cut},\ \forall\ t \in T \quad (8)$$

$$0 \le p_t^{b,+} \le \overline{P}^{AC,+}\delta_t^b,\ \forall\ t \in T \quad (9)$$

$$0 \le p_t^{b,-} \le \overline{P}^{AC,-}(1-\delta_t^b),\ \forall\ t \in T \quad (10)$$

$$\begin{cases} e_t^b = \hat{e}^{b,0} + \left(p_t^{b,+}\hat{\eta}^{b,+} - \frac{p_t^{b,-}}{\hat{\eta}^{b,-}}\right)\Delta t,\ t = 1 \\ e_t^b = e_{t-1}^b + \left(p_t^{b,+}\hat{\eta}^{b,+} - \frac{p_t^{b,-}}{\hat{\eta}^{b,-}}\right)\Delta t,\ t \in]1,T] \end{cases} \quad (11)$$

$$\underline{E}^b \le e_t^b \le \overline{E}^b \quad (12)$$

$$e_t^{PCC}\frac{1}{\Delta t} = p_t^{abs} + p_t^{inj},\ \forall\, t \in T \tag{13}$$

$$\Delta e_t^- - \Delta e_t^+ = e_t^{PCC} + e_t^{DA},\ \forall\, t \in T, \Delta e_t^-, \Delta e_t^+ \in \mathbb{R}_0^+ \tag{14}$$

A. *Wind-solar hybrid parks*

Often it is required of HP to comply with a certain $tg(\phi) > 0$ at the point of common coupling (PCC). Including apparent power flows and the possibility for BESS to discharge reactive power, introduces a non-linearity in the problem. The P-Q capability curve, establishing the relationship between apparent, active and reactive powers that can be discharged at each step, is a quadratic equation and must therefore be duly linearized. We opted for a trapezium-based technique, as described in [16], where the P-Q capability curve is approximated by a series of trapezium shapes, as shown in Fig. 4. The trapeziums are bounded by fractions of the inverter's apparent power and can be unevenly distributed to minimize the approximation error. Only the first quadrant of the P-Q capability curve is approximated since we are only considering injection of reactive power, which can occur when $p_t^{b,-} > 0$.

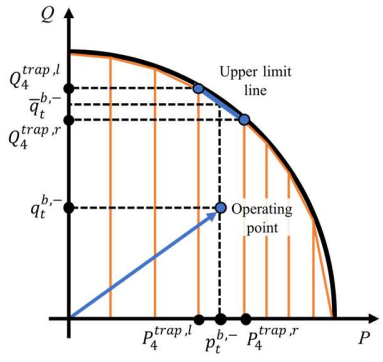

Figure 4. Approximation of the P-Q capability curve (1st quadrant) by a trapeziums-based technique. An example is depicted where the operating point is framed by the limits of the 4th trapezium. Adapted from [16].

The supplementary restrictions for HP are the following (note: in (15), $tg(\hat{\phi})_t$ is the Q/P injection ratio at the PCC, during t and $\hat{\phi}^G$ is the RES generation plants' power factor; in (19), $\widehat{M}$ is a very large positive number):

$$tg(\hat{\phi})_t p_t^{inj} = \sum_{z\in Z} q_{z,t}^{b,tr} + tg\left(cos^{-1}(\hat{\phi}^G)\right)(\hat{P}_t^G - p_t^{G,cut}),\ \forall\, t \in T \tag{15}$$

$$p_t^{b,-} = \sum_{z\in Z} p_{z,t}^{b,tr},\ \forall\, t \in T \tag{16}$$

$$\delta_{z,t}^{b,tr}\hat{P}_z^{tr,l} \le p_{z,t}^{b,tr} \le \delta_{z,t}^{b,tr}\hat{P}_z^{tr,r},\ \forall\, z \in Z,\ t \in T \tag{17}$$

$$q_{z,t}^{b,tr} \le \hat{Q}_z^{tr,l} + \frac{\hat{Q}_z^{tr,r} - \hat{Q}_z^{tr,l}}{\hat{P}_z^{tr,r} - \hat{P}_z^{tr,l}}\left(p_t^{b,-} - \hat{P}_z^{tr,l}\right),\ \forall\, z \in Z,\ t \in T \tag{18}$$

$$0 \le q_{z,t}^{b,tr} \le \widehat{M}\delta_{z,t}^{b,tr},\ \forall\, z \in Z,\ t \in T \tag{19}$$

$$\sum_{z\in Z} \delta_{z,t}^{b,tr} = 1,\ \forall\, t \in T. \tag{20}$$

B. *Microgrids*

Instead of considering the possibility of having to comply with a certain $tg(\phi) > 0$ at the PCC, which is not common for MG systems, other constraints must be added regarding load curtailment. The MILP general formulation includes the possibility to consider flexible and inflexible loads for these systems. Of the first, this work only considers curtailable loads, i.e., the total demand can be curtailed at each time step restricted to some time conditions, but a rebound effect is not considered. The time conditions applied include a maximum downtime ($\hat{T}^{MD}$) followed by a minimum uptime ($\hat{T}^{mU}$).

Equation (21) establishes the curtailed power at each time step t, provided the load is available for curtailment ($\hat{\delta}_t^{flex} = 1$) and that the time constraints are met. Inflexible loads can be modelled by setting $\hat{\delta}_t^{flex} = 0,\ \forall\, t \in T$. Constraints (22) and (23) establish the time conditions along the optimization horizon. Constraint (24a) addresses the conditions at the beginning of the optimization horizon. The number of consecutive time steps t that the curtailable load must remain being provided (T^U) or can remain curtailed (T^D) are calculated beforehand through (24b). For these calculations, the number of previous, consecutive steps the load has been provided ($\hat{T}^{U0}$) or curtailed ($\hat{T}^{D0}$) at $t = 1$ and its initial status $\hat{\delta}^{L,0}$ (0: curtailed, 1: provided) are required. Finally, (25) establishes the minimum uptime condition at the end of the optimization horizon.

$$p_t^{L,cut} = \hat{\delta}_t^{flex}(1 - \delta_t^L)\hat{P}_t^L,\ \forall\, t \in T \tag{21}$$

$$\sum_t^{t+\hat{T}^{mU}-1} \delta_t^L \ge \hat{T}^{mU}(\delta_t^L - \delta_{t-1}^L),\ \forall\, t \in \{1, \dots, T - \hat{T}^{mU}\} \tag{22}$$

$$\sum_t^{t+\hat{T}^{MD}} \delta_t^L \ge \delta_{t-1}^L - \delta_t^L,\ \forall\, t \in \{1, \dots, T - \hat{T}^{MD}\} \tag{23}$$

$$\begin{cases} \sum_{t=1}^{T^U}(1 - \delta_t^L) = 0, & if\ \hat{\delta}^{L,0} = 1 \\ \sum_{t=1}^{T^D+1} \delta_t^L \ge 1, & if\ \hat{\delta}^{L,0} = 0 \end{cases} \tag{24a}$$

$$\begin{cases} T^U = max\left[\left(\hat{T}^{mU} - \hat{T}^{U0}\right), 0\right]\hat{\delta}^{L,0} \\ T^D = max\left[\left(\hat{T}^{MD} - \hat{T}^{D0}\right), 0\right]\left(1 - \hat{\delta}^{L,0}\right) \end{cases} \tag{24b}$$

$$\sum_t^T \delta_t^L \geq (T-t+1)(\delta_t^L - \delta_{t-1}^L),\ \forall\, t > T - \hat{T}^{mU} \quad (25)$$

C. Considering a limit to BESS daily degradation

To consider a daily limit to BESS degradation, as explained in section II.C., (26) must be included in the MILP formulation. Since the algorithm was designed to be implemented within an MPC framework, if $T > 12h$, the optimization horizon of MILPs at a certain iteration of the MPC will encompass not only steps within the day being optimized ($t \in T^1$), but also steps of the next day ($t \in T^2$). Please note that $\{T^1, T^2\} = T$ and that if $T \leq 12h \Rightarrow T^1 = T$. e_t^{deg} needs to be reset for $t \in T^2$ which is achieved by implementing (27). Note that the BESS degradation since t=1, $\hat{E}^{deg,T^1}$, is given by previous iterations of the MPC.

$$\sum_t^{T^1} e_t^{deg} \leq \overline{E}^{deg} - \hat{E}^{deg,T^1} \quad (26)$$

$$\sum_t^{T^2} e_t^{deg} \leq \overline{E}^{deg} \quad (27)$$

D. Considering V-I characteristics

To consider variable energy content limits, (12) must be replaced by (28).

$$\hat{m}^{b,-}\frac{p_t^{b,-}}{\hat{\eta}^{b,-}} + \hat{o}^{b,-} \leq e_t^b \leq \hat{m}^{b,+} p_t^{b,+} \hat{\eta}^{b,+} + \hat{o}^{b,+},\ \forall\, t \in T \quad (28)$$

E. Considering a linear approximation to the inverter's efficiency curve

First, the terms $p_t^{b,+}\hat{\eta}^{b,+}$ and $\frac{p_t^{b,-}}{\hat{\eta}^{b,-}}$ at (11) and (28) must be substituted by $\sum_s z_{t,s}^{b,+}$ and $\sum_s z_{t,s}^{b,-}$, respectively. Next, (9) and (10) must be substituted by (29) and (30), respectively.

$$\underline{P}_s^{b,+}\delta_{t,s}^{b,+} \leq p_{t,s}^{b,+} \leq \overline{P}_s^{b,+}\delta_{t,s}^{b,+},\ \forall\, t \in T, s \in S \quad (29)$$

$$\underline{P}_s^{b,-}\delta_{t,s}^{b,-} \leq p_{t,s}^{b,-} \leq \overline{P}_s^{b,-}\delta_{t,s}^{b,-},\ \forall\, t \in T, s \in S \quad (30)$$

Additionally, the following constraints must be considered:

$$z_{t,s}^{b,+} = \frac{1}{\hat{m}^{\eta,+}}(p_{t,s}^{b,+} - \hat{o}^{\eta,+}\delta_{t,s}^{b,+}),\ \forall\, t \in T, s \in S \quad (31)$$

$$z_{t,s}^{b,-} = \frac{1}{\hat{m}^{\eta,-}}(p_{t,s}^{b,-} - \hat{o}^{\eta,-}\delta_{t,s}^{b,-}),\ \forall\, t \in T, s \in S \quad (32)$$

$$\sum_s\left(\delta_{t,s}^{b,+} + \delta_{t,s}^{b,-}\right) \leq 1,\ \forall\, t \in T, s \in S. \quad (33)$$

Note that (31) and (32), for a constant segment, must be defined as $p_{t,s}^{b,+/-} = \hat{o}^{\eta,+/-}\delta_{t,s}^{b,+/-}$, respectively, since $\hat{m}^{\eta,+/-} = 0$.

IV. Case Study and Results

The algorithms were implemented in Python, using the linear programming modeler puLP [17] and the default COIN-OR Branch-and-Cut solver [18] setting the mipgap to 1E-3. The performance tests were conducted on a Laptop PC with AMD® Ryzen® CPU 5 PRO 4650U @2.10 GHz and a 16GB RAM.

To evaluate the impact of considering a constrained BESS usage by limiting its daily degradation, 8 scenarios were prepared, combining the adopted strategy (conservative versus unconstrained BESS usage) with each system type (HP or MG) and each objective function presented (price arbitrage - OF1 or minimizing energy deviations - OF2). Both systems were configured with a total of 10 MWp of RES and a 5 MWh BESS. For the constrained scenarios, we considered the BESS desired lifetime to be 10 years and EOL = 70%. The MG has a peak demand of 10 MVA, of which 25% is curtailable. For this simulation, we considered that all assets remain active throughout the year, i.e., no maintenance is defined.

The simulations performed over the 8 scenarios were supported by hourly data spanning a total of one year. PV forecasts were adapted from real measurements obtained from panels installed at INESC TEC main building's rooftop in Porto, Portugal [19]. Load forecasts were adapted from energy consumption readings from households participating in the Low Carbon London project [20] (data available at [21]). Historical spot market prices of MIBEL [22] were used and feed-in tariffs were estimated as a variable, inferior percentage of those prices. For OF2, day-ahead bids were simulated by adding gaussian white noise to the forecasted net load so that the mean absolute percentage error (MAPE) between day-ahead bids and forecasts was roughly 10% (a value in par with current state-the-art forecasting tools' MAPE for load demand [23] and RES generation [24]). For the HP, a $tg(\hat{\phi})_t = 0.3$ was established at peak consumption hours, distinguishing between the summer and winter seasons and between working days and weekends, according to the Portuguese energy regulation entity ERSE [25].

A sensitivity analysis was first carried out for the frameworks' performance and computational efficiency. Table I summarizes the average time required for the MILPs to reach an optimal solution for the 8 different scenarios over the year. Generally, the proposed model leads to an increase in the average optimization time, as expected. Nonetheless, the times presented are adequate for real-time applications relying on non-commercial solvers, thus enabling the implementation of an MPC framework. This is further supported when considering that load curtailment (for the MG) and reactive set points (for the HP) increase the computational weight of the problem.

BESS Model	System	Obj. Func.	Time (average)
Enhanced	HP	OF1	2,806 s
		OF2	0,651 s
	MG	OF1	3,010 s

		OF2	0,386 s
Simple	HP	OF1	0,340 s
		OF2	0,308 s
	MG	OF1	0,155 s
		OF2	0,160 s

AVERAGE OPTIMIZATION TIMES FOR DIFFERENT SCENARIOS.

The algorithms' performance when considering the enhanced BESS model, on systems with increasing size, was also evaluated. For this purpose, a HP and a MG with 10 BESS, 10 RES plants and 10 load assets, 50% of which are curtailable were defined. A day in the data set with high generation and consumption fluctuations was selected for a series of trial runs on both systems, including the two objective functions and different horizons (6h, 12h and 24h), and timesteps (5', 15' and 60'). To comply with the smaller steps, the data was resampled (original load forecasts had a 30' step while generation, market and feed-in data had a 1h step). Three independent runs were performed for each combination to determine an average performance, as shown in Fig. 5. The optimization problem could not be solved within a time limit of 5 minutes for scenario HP_OF2 considering a 24h horizon and a 5' step. As such, this scenario was excluded from the results in Fig. 5. All other scenarios where successfully run and optimally solved under 3 minutes, which reinforces the adequacy of the algorithm for real-time applications. The comparison between results for the 24h horizon, 60-minute step scenarios with the average time values at Table I, shows that there is no significant impact on the optimization time from considering more assets.

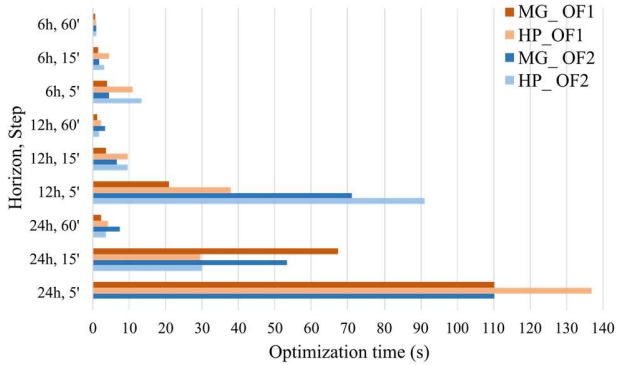

Figure 5. Optimization time comparison between different system, objective function, horizon and step scenarios for more complex systems.

The impact of using a conservative versus an unconstrained strategy on the values obtained for OF1 and OF2, on both systems, was analyzed considering one-year simulations over the 8 scenarios described earlier. The results are summarized at Table II. Given the low error between the day-ahead bids and forecasts, no major differences were observed for OF2. Nonetheless, it is worth highlighting that the conservative strategy achieved close to 1% less deviations in the simulated year for the MG. Conversely, a conservative strategy with OF1 leads to a positive impact on BESS degradation and a negative impact on the expected revenues. For the HP, this value decreases 0,73% but with a benefit of 23,42% less degradation. For the MG, the value decreases 27,45%, linked to a decrease in BESS degradation of 17,65%. Clearly, there is a tradeoff between liquid profitability and an increased BESS lifetime which we can argue to depend on multiple factors such as the system and its configured assets, the adequacy of the BESS installed capacity, the objective function and the quality of the forecasts used in the algorithm (i.e., for OF2, more accurate forecasts imply more accurate bids and a lesser need to use the flexibility of the BESS).

System	Obj. Func.	Percentual difference	
		Obj. Func. Value	*Degradation*
HP	OF1	- 0,73 %	- 23,42 %
	OF2	0,00 %	0,00 %
MG	OF1	- 27,45 %	- 17,65 %
	OF2	- 0,94 %	0,00 %

PERCENTUAL DIFFERENCE IN OBJECTIVE FUNCTION VALUES AND TOTAL DEGRADATION BETWEEN BESS USAGE STRATEGIES.

V. DISCUSSION

A tractable BESS linear model was proposed in this work able to be integrated in a MILP framework. The model can be described by analytical and explicit expressions, is easily calibrated, with its parameters being obtained by either recurring to manufacturers' datasheets or through relatively simple tests. Additionally, the model is based on power setpoints which, excluding losses, are constant as opposed to voltage and current setpoints that can vary in different parts of the asset. The tractability of the model is met on the other hand by a decrease in its accuracy, given the considerations and simplifications required. A first consideration established is that the voltage is a good indicator of the energy content of a Li-ion battery, but this is only true when the battery is in an idle state. In that regard, while the (dis)charge events are assumed to be performed at the beginning of an optimization step, the energy content is estimated at the end of that step, where we can assume an idle state for the BESS. Another simplification considered is the immutability of the BESS parameters, namely its' degradation dynamics and energy content throughout the optimization horizon but, at such timescales (6-24h), no significant impact would be imposed in the optimization procedure. Furthermore, the BESS parameters can always be updated between runs as more information at the Battery Management System (BMS) becomes available.

Considering the approximation for the BESS efficiency, one can argue that it can still introduce a significant error, which can be mitigated by defining other steps between intermediate thresholds and approximating the higher rated powers by a line and not a constant. Naturally, such considerations come at the cost of computational tractability.

The simulations where BESS usage was constrained by a daily degradation limit highlighted the influence of 1) the adequacy of the installed capacities to the configured system; 2) the restrictiveness to be imposed on the daily degradation, and 3) the cost attributed to BESS degradation, whose definition resides outside the scope of this work. In practical applications, we recommend the BESS degradation curve to be updated from time to time. Further tests with real BESS need to be performed to identify the periodicity of such updates.

Finally, the simulation times obtained with non-commercial solvers allow to infer that the model presented is well suited for real-time operation of either system. There is the possibility of considering multiple asset types, thus resulting in an increased system complexity, without significantly impacting the simulation time, enabling the extension of the model to the MPC framework. A bottleneck of this methodology can however be identified in the total number of optimization steps considered. For time steps smaller than 15 minutes, some scenario combinations were not solved within the time limit, which might be overcome with more powerful solvers.

VI. CONCLUSIONS

This work presented an optimization framework apt for real-time operation of small electrical systems such as microgrids or hybrid parks. The main novelty of this work resides in introducing a linear model for BESS, based on three fundamental pillars (VI-characteristics, system efficiency and degradation estimation), that is more accurate than widely used naïve models, but also tractable enough to not compromise its application in real-time control frameworks. The results highlighted have not only supported this conclusion but have also shown the importance of studying and anticipating BESS degradation since it can have a major impact on the expected operation costs/revenues on those systems.

REFERENCES

[1] B. Heymann, J. F. Bonnans, P. Martinon, F. J. Silva, F. Lanas, and G. Jiménez-Estévez, "Continuous optimal control approaches to microgrid energy management," Energy Syst, vol. 9, no. 1, pp. 59–77, Feb. 2018, doi: 10.1007/s12667-016-0228-2.

[2] X. Wu, W. Zhao, X. Wang, and H. Li, "An MILP-Based Planning Model of a Photovoltaic/Diesel/Battery Stand-Alone Microgrid Considering the Reliability," IEEE Transactions on Smart Grid, vol. 12, no. 5, pp. 3809–3818, Sep. 2021, doi: 10.1109/TSG.2021.3084935.

[3] M. Andrychowicz, "The Impact of Energy Storage along with the Allocation of RES on the Reduction of Energy Costs Using MILP," Energies, vol. 14, no. 13, Art. no. 13, Jan. 2021, doi: 10.3390/en14133783.

[4] M. Farrokhifar, F. H. Aghdam, A. Alahyari, A. Monavari, and A. Safari, "Optimal energy management and sizing of renewable energy and battery systems in residential sectors via a stochastic MILP model," Electric Power Systems Research, vol. 187, p. 106483, Oct. 2020, doi: 10.1016/j.epsr.2020.106483.

[5] P. Liu, Z. Cai, P. Xie, X. Li, and Y. Zhang, "A Computationally Efficient Optimization Method for Battery Storage in Grid-connected Microgrids Based on a Power Exchanging Process," Energies, vol. 12, no. 8, Art. no. 8, Jan. 2019, doi: 10.3390/en12081512.

[6] T. Pippia, J. Sijs, and B. De Schutter, "A Single-Level Rule-Based Model Predictive Control Approach for Energy Management of Grid-Connected Microgrids," IEEE Transactions on Control Systems Technology, vol. 28, no. 6, pp. 2364–2376, Nov. 2020, doi: 10.1109/TCST.2019.2945023.

[7] P. Siano and D. Mohammad, "MILP Optimization model for assessing the participation of distributed residential PV-battery systems in ancillary services market," CSEE Journal of Power and Energy Systems, vol. 7, no. 2, pp. 348–357, Mar. 2021, doi: 10.17775/CSEEJPES.2020.01170.

[8] D. T. Vedullapalli, R. Hadidi, and B. Schroeder, "Combined HVAC and Battery Scheduling for Demand Response in a Building," IEEE Transactions on Industry Applications, vol. 55, no. 6, pp. 7008–7014, Nov. 2019, doi: 10.1109/TIA.2019.2938481.

[9] Y. Li and J. Wu, "Optimum Integration of Solar Energy With Battery Energy Storage Systems," IEEE Transactions on Engineering Management, pp. 1–11, 2020, doi: 10.1109/TEM.2020.2971246.

[10] R. C. Guerrero, M. Angelo, and A. Pedrasa, "An MILP-Based Model for Hybrid Renewable Energy System Planning Considering Equipment Degradation and Battery Lifetime," in 2019 IEEE 2nd International Conference on Power and Energy Applications (ICPEA), Apr. 2019, pp. 207–211. doi: 10.1109/ICPEA.2019.8818521.

[11] M. A. Hannan et al., "Battery energy-storage system: A review of technologies, optimization objectives, constraints, approaches, and outstanding issues," Journal of Energy Storage, vol. 42, p. 103023, Oct. 2021, doi: 10.1016/j.est.2021.103023.

[12] J. M. Reniers, G. Mulder, S. Ober-Blöbaum, and D. A. Howey, "Improving optimal control of grid-connected lithium-ion batteries through more accurate battery and degradation modelling," Journal of Power Sources, vol. 379, pp. 91–102, Mar. 2018, doi: 10.1016/j.jpowsour.2018.01.004.

[13] F. Kazhamiaka, C. Rosenberg, S. Keshav, and K.-H. Pettinger, "Li-ion storage models for energy system optimization: the accuracy-tractability tradeoff," Jun. 2016, pp. 1–12. doi: 10.1145/2934328.2934345.

[14] F. Kazhamiaka, C. Rosenberg, and S. Keshav, "Tractable lithium-ion storage models for optimizing energy systems," Energy Informatics, vol. 2, no. 1, p. 4, May 2019, doi: 10.1186/s42162-019-0070-6.

[15] J. Solano, "Energy And Economic Optimization Of Pv Hybrid Systems To Supply Buildings Hvac Demand: Battery Modeling And Control Strategies," 2018. doi: 10.20868/UPM.thesis.50457.

[16] A. Hamidi, S. Golshannavaz, and D. Nazarpour, "D-FACTS Cooperation in Renewable Integrated Microgrids: A Linear Multiobjective Approach," IEEE Transactions on Sustainable Energy, vol. 10, no. 1, pp. 355–363, Jan. 2019, doi: 10.1109/TSTE.2017.2723163.

[17] pulp. COIN-OR Foundation, 2021. Accessed: Sep. 08, 2021. [Online]. Available: https://github.com/coin-or/pulp

[18] Cbc. COIN-OR Foundation, 2021. Accessed: Sep. 08, 2021. [Online]. Available: https://github.com/coin-or/Cbc

[19] G. P. Monteiro, A. I. Palmero-Marrero, C. Moreira, and A. C. Oliveira, "Evaluation of the performance of a photovoltaic power plant installed in a building in the north of Portugal," Energy Procedia, vol. 153, pp. 42–47, Oct. 2018, doi: 10.1016/j.egypro.2018.10.033.

[20] "UK Power Networks - Low Carbon London," UK Power Networks. https://innovation.ukpowernetworks.co.uk/projects/low-carbon-london/ (accessed Sep. 30, 2021).

[21] "SmartMeter Energy Consumption Data in London Households - London Datastore." https://data.london.gov.uk/dataset/smartmeter-energy-use-data-in-london-households (accessed Sep. 30, 2021).

[22] "SIMEE - Daily and Intraday - Prices." https://www.mercado.ren.pt/EN/Electr/MarketInfo/MarketResults/OMIE/Pages/Prices.aspx (accessed Sep. 08, 2021).

[23] A. A. Mamun, Md. Sohel, N. Mohammad, Md. S. Haque Sunny, D. R. Dipta, and E. Hossain, "A Comprehensive Review of the Load Forecasting Techniques Using Single and Hybrid Predictive Models," IEEE Access, vol. 8, pp. 134911–134939, 2020, doi: 10.1109/ACCESS.2020.3010702.

[24] R. Ahmed, V. Sreeram, Y. Mishra, and M. D. Arif, "A review and evaluation of the state-of-the-art in PV solar power forecasting: Techniques and optimization," Renewable and Sustainable Energy Reviews, vol. 124, p. 109792, May 2020, doi: 10.1016/j.rser.2020.109792.

[25] "ERSE - Tarifas e preços - eletricidade." https://www.erse.pt/atividade/regulacao/tarifas-e-precos-eletricidade/#periodos-horarios (accessed Oct. 02, 2021).